PHYSICAL REVIEW B **91**, 081302(R) (2015)

Split Dirac cones in HgTe/CdTe quantum wells due to symmetry-enforced level anticrossing at interfaces

S. A. Tarasenko,[1] M. V. Durnev,[1] M. O. Nestoklon,[1] E. L. Ivchenko,[1] Jun-Wei Luo,[2,3] and Alex Zunger[4]

[1]*Ioffe Physical-Technical Institute, 194021 St. Petersburg, Russia*

[2]*State Key Laboratory of Superlattices and Microstructures, Institute of Semiconductors, Chinese Academy of Sciences, Beijing 100083, China*

[3]*Synergetic Innovation Center of Quantum Information and Quantum Physics, University of Science and Technology of China, Hefei, Anhui 230026, China*

[4]*University of Colorado, Boulder, Colorado 80309, USA*

(Received 12 November 2014; revised manuscript received 27 January 2015; published 18 February 2015)

HgTe is a band-inverted compound which forms a two-dimensional topological insulator if sandwiched between CdTe barriers for a HgTe layer thickness above the critical value. We describe the fine structure of Dirac states in the HgTe/CdTe quantum wells of critical and close-to-critical thicknesses and show that the necessary creation of interfaces brings in another important physical effect: the opening of a significant anticrossing gap between the tips of the Dirac cones. The level repulsion driven by the natural interface inversion asymmetry of zinc-blende heterostructures considerably modifies the electron states and dispersion but preserves the topological transition at the critical thickness. By combining symmetry analysis, atomistic calculations, and extended $\boldsymbol{k}\cdot\boldsymbol{p}$ theory with interface terms, we obtain a quantitative description of the energy spectrum and extract the interface mixing coefficient. We discuss how the fingerprints of the predicted zero-magnetic-field splitting of the Dirac cones could be detected experimentally by studying magnetotransport phenomena, cyclotron resonance, Raman scattering, and THz radiation absorption.

DOI: 10.1103/PhysRevB.91.081302 PACS number(s): 73.20.−r, 73.21.Fg, 73.63.Hs, 78.67.De

The study of systems with gapless and linear-dispersion states constituting the Dirac cone is central to the physics of topological insulators (TIs) [1,2]. Such states are formed in the primary insulating band gap of a bulk material and studied at the surface via techniques such as angular resolved photoemission [3,4]. While some TI compounds such as Bi_2Se_3 and Bi_2Te_3 show an insulating gap in their three-dimensional (3D) bulk band structure and so the Dirac cones can be studied at their two-dimensional (2D) surface without modifying the material, a mercury telluride crystal does not have a 3D bulk band gap because the Fermi level resides within the fourfold degenerate Γ_8 band [5]. However, topological insulation is realized by straining HgTe, which opens a gap within the otherwise fourfold degenerate Γ_8 states [6,7] or growing the material in a HgTe/CdTe quantum well (QW) geometry [8–10]. In the latter case, CdTe (or $Cd_{1-x}Hg_xTe$) barriers create quantum confinement within HgTe with the normal or inverted band structure depending on the well thickness, so that HgTe/CdTe QWs belong to the class of normal or topological insulators.

In HgTe/CdTe QWs of critical thickness, the heavy-hole subband $HH1$ switches order with the electron subband $E1$ [11], the band gap vanishes, and elementary excitations behave as massless Dirac 2D fermions [12,13]. An early theoretical description [8] used a model in which the symmetry of the HgTe/CdTe QW was implicitly assumed to contain an inversion center. Consequently, the point-group representations of the $E1$ and $HH1$ subbands are different, so these states do not mix with each other and are allowed to cross. In reality, the host zinc-blende structures lack an inversion center and the QW structure has a further reduced symmetry compared to the bulk materials, even if the interfaces are lattice matched and defect free, and the well is symmetric. Indeed, each of the two (001) interfaces possesses a C_{2v} symmetry and taken together the symmetric well has a D_{2d} symmetry. It is known from analogous GaAs/AlAs QW structures that, in the D_{2d} group, the $E1$ and $HH1$ states transform according to the same spinor representations [14–16]. Therefore, the coupling matrix element between $E1$ and $HH1$ is nonzero, and these subbands must anticross rather than cross at zero in-plane wave vector $\boldsymbol{k}$. As pointed out in Refs. [17–20], in the case of HgTe/CdTe QWs, a reduction in symmetry leads to a splitting of states at $\boldsymbol{k}=\boldsymbol{0}$. However, a theory identifying the source of the splitting (bulk versus interface) and predicting its magnitude has been lacking. Experimental data on weak localization and Shubnikov–de Haas oscillations also indicate strong spin-orbit splitting of the states [21]. Here, we present a microscopic theory of the Dirac states in HgTe/CdTe QWs that predicts a very large (∼15 meV) anticrossing gap between the tips of the Dirac cones in QWs of a critical thickness. We find that this splitting is predominantly due to the interfacial $E1-HH1$ repulsion mandated by the physical D_{2d} symmetry, which is missed by naive continuum-medium considerations but seen when theory acquires atomic resolution. Using this picture we further provide a detailed analysis of the fine structure of Dirac states, which is a key to understanding transport phenomena. As the main result, Fig. 1 shows the energy spectra in QWs of (a) a critical thickness $d=d_c$ and (b) close-to-critical thickness $d\neq d_c$. Even in symmetric structures of the critical thickness, the Dirac states are split at the zone center and the spectrum consists of two cones shifted vertically with respect to each other. For $d\neq d_c$, the spectrum becomes more complex: It has a gap and extrema on a circle in the momentum space. We analyze the nature of anticrossing, obtain a quantitative description of the energy spectrum, and discuss the consequences of the splitting on the transport and optical properties of QWs.

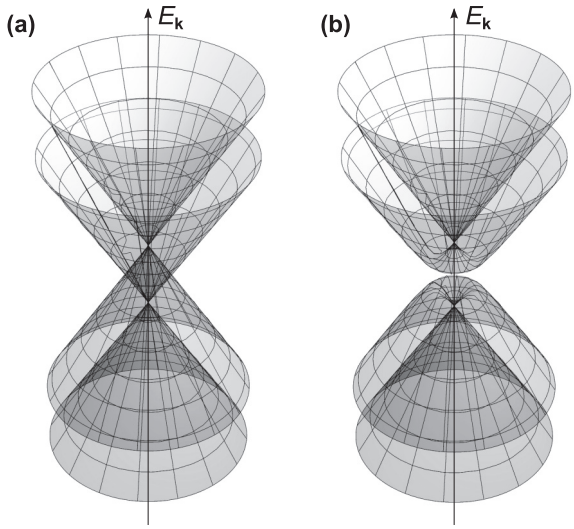

FIG. 1. Energy spectra of HgTe/CdHgTe QWs of (a) the critical and (b) close-to-critical thicknesses. The spectra are plotted after Eq. (3) for (a) $\delta = 0$ and (b) $\delta = \gamma/2$.

Mechanisms leading to splitting in QWs with a symmetric confinement potential originate fundamentally from bulk inversion asymmetry of the host crystal and interface inversion asymmetry. The relative importance of these contributions cannot be deduced from model Hamiltonian considerations. Atomistic descriptions, on the other hand, capture accurately the relevant asymmetry via the specification of atomic types and positions.

Figures 2 and 3 show the results of atomistic calculations of the energy spectrum of HgTe/CdTe QWs obtained in the screened plane-wave pseudopotential and tight-binding theories, respectively. The pseudopotential method is described in Ref. [10]; details of the tight-binding calculations are given in the Supplemental Material [22]. The subband arrangement as a function of the QW width at $\boldsymbol{k} = \boldsymbol{0}$ is presented in Figs. 2(a), 2(b), and 3(a). Both the pseudopotential and

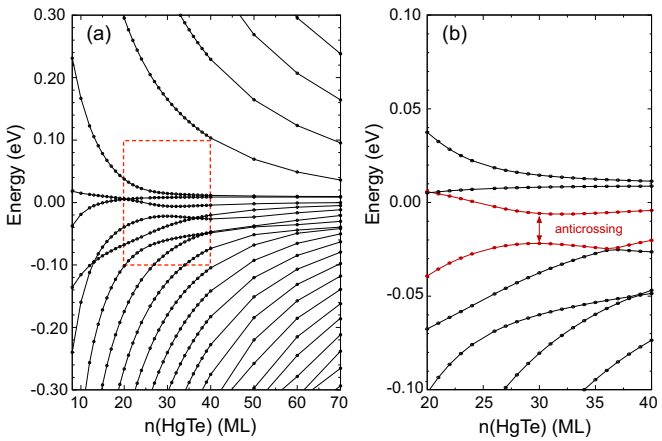

FIG. 2. (Color online) (a) Arrangement of energy subbands in (001) $(HgTe)_n/(CdTe)_{40}$ QW structures as a function of the number of HgTe monolayers (ML) obtained by the pseudopotential method. (b) Zoom in of the anticrossing area.

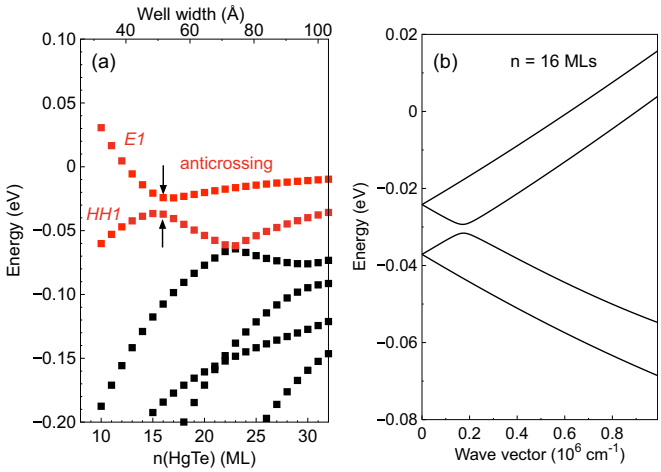

FIG. 3. (Color online) (a) Arrangement of energy subbands in (001) $(HgTe)_n$/CdTe QW structures as a function of the number of HgTe monolayers obtained by the sp^3 tight-binding method. (b) Electron dispersion $E(\boldsymbol{k})$ in the 16-ML-wide QW.

tight-binding calculations yield a wide anticrossing gap between the electronlike $E1$ and heavy-hole $HH1$ subbands at the Γ point. The two approaches give different values of the critical QW width because of the sensitivity of the subband structure to the model. Indeed, the pseudopotential calculation reveals, for the QW structures, interface-localized bands located energetically between $E1$ and the $HH1$ state (see Ref. [10]). Nevertheless, all calculations that acknowledge the atomistic symmetry—as opposed to a continuum view—do give a large anticrossing at the critical QW thickness. They both predict a gap of about 15 meV, far exceeding the estimate of a few meV due solely to the bulk inversion asymmetry [18,19] and unambiguously indicating that the subband mixing is dominated by the interface contribution, in a crucial difference from the naive $\boldsymbol{k}\cdot\boldsymbol{p}$ model. Moreover, despite the existence of additional interface bands in the pseudopotential calculation, both models predict the same dispersion of the Dirac states formed from the $E1$ and $HH1$ subbands near the anticrossing point.

Figure 3(b) demonstrates the energy dispersion $E(\boldsymbol{k})$ of the coupled $E1$ and $HH1$ states calculated by the tight-binding method for a well width of 16 monolayers, which is very close to the critical thickness. The exact condition $d = d_c$ cannot be fulfilled in structures with an integer number of monolayers. The spectrum consists of four almost linearly dispersed branches which are split at $k = 0$. The slope of the branches yields a velocity 6.1×10^7 cm/s, which is close to the electron velocity 7.2×10^7 cm/s [13] and 6.4×10^7 cm/s [23] determined by cyclotron resonance in HgTe/HgCdTe QWs of critical thickness. The two middle-energy branches anticross at the finite wave vector $k_0 \approx 0.17 \times 10^6$ cm^{-1} with the energy gap being highly sensitive to the deviation of QW width d from d_c. In QWs with $d \approx d_c$ [Fig. 3(b)], this gap is far smaller than the splitting at $k = 0$.

Inspired by the atomistic results, we now present an effective model Hamiltonian—the atomically inspired $\boldsymbol{k}\cdot\boldsymbol{p}$ model (AIKP)—which takes into account the correct D_{2d} symmetry of the quantum well. We limit the AIKP model

to four basis Bloch state functions forming the Dirac states. Such an approach is valid as long as the anticrossing gap at $\boldsymbol{k} = \mathbf{0}$ is smaller than the energy separation from the coupled $E1 - HH1$ subbands to other excited subbands. The basis functions have the form [8]

$$\begin{aligned} |E1, +1/2\rangle &= f_1(z)|\Gamma_6, +1/2\rangle + f_4(z)|\Gamma_8, +1/2\rangle, \\ |HH1, +3/2\rangle &= f_3(z)|\Gamma_8, +3/2\rangle, \\ |E1, -1/2\rangle &= f_1(z)|\Gamma_6, -1/2\rangle + f_4(z)|\Gamma_8, -1/2\rangle, \\ |HH1, -3/2\rangle &= f_3(z)|\Gamma_8, -3/2\rangle, \end{aligned} \tag{1}$$

where $f_1(z)$, $f_3(z)$, and $f_4(z)$ are the envelope functions, z is the growth direction, and $|\Gamma_6, \pm 1/2\rangle$, $|\Gamma_8, \pm 1/2\rangle$, and $|\Gamma_8, \pm 3/2\rangle$ are the basis functions of the Γ_6 and Γ_8 states at the Γ point of the Brillouin zone, respectively. The 4×4 effective Hamiltonian describing the coupling at a finite in-plane wave vector $\boldsymbol{k}$ can be constructed by using the theory of group representations. Taking into account that, in the D_{2d} point group, the states $|E1, \pm 1/2\rangle$ and $|HH1, \mp 3/2\rangle$ transform according to the spinor representation Γ_6 while the wave vector components k_x,k_y belong to the irreducible representation Γ_5, one derives the effective Hamiltonian to first order in the wave vector as

$$H = \begin{pmatrix} \delta & iAk_+ & 0 & i\gamma \\ -iAk_- & -\delta & i\gamma & 0 \\ 0 & -i\gamma & \delta & -iAk_- \\ -i\gamma & 0 & iAk_+ & -\delta \end{pmatrix}, \tag{2}$$

where A, δ, and γ are linearly independent parameters, $k_\pm = k_x \pm ik_y$, and $x \parallel [100]$ and $y \parallel [010]$ are the in-plane axes. The value 2δ stands for the energy spacing between the $E1$ and $HH1$ subbands in the absence of mixing; δ can be tuned from a positive to negative value by varying the QW thickness d. In particular, $\delta = 0$ for the critical thickness $d = d_c$ [11]. The parameter A determines the velocity of Dirac fermions. In the $\boldsymbol{k}\cdot\boldsymbol{p}$ model, it is given by $A = (P/\sqrt{2}) \int f_1(z) f_3(z) dz + \delta A$, where P is the Kane matrix element and δA stands for the contributions from remote bands. Finally, γ describes the coupling of $E1$ and $HH1$ states at $\boldsymbol{k} = \mathbf{0}$ in zinc-blende-lattice QWs [18,19], $2|\gamma| \approx 15$ meV, as it follows from Figs. 2 and 3, neglecting the influence of additional interface states.

The solution of the secular equation for the matrix Hamiltonian (2) yields the energy spectrum

$$E_{1,4} = \mp\sqrt{\delta^2 + (Ak + \gamma)^2}, \quad E_{2,3} = \mp\sqrt{\delta^2 + (Ak - \gamma)^2}. \tag{3}$$

The corresponding wave functions are given by

$$\Psi_{1,4} = \frac{1}{2}\begin{pmatrix} a_{1,4} \\ b_{1,4}\, e^{-i\varphi} \\ -a_{1,4}\, e^{-i\varphi} \\ b_{1,4} \end{pmatrix}, \quad \Psi_{2,3} = \frac{1}{2}\begin{pmatrix} a_{2,3} \\ b_{2,3}\, e^{-i\varphi} \\ a_{2,3}\, e^{-i\varphi} \\ -b_{2,3} \end{pmatrix}, \tag{4}$$

where $a_{1,2} = -i\sqrt{(E_{1,2} + |\delta|)/E_{1,2}}\,\mathrm{sgn}(Ak \pm \gamma)$, $b_{1,2} = \sqrt{(E_{1,2} - |\delta|)/E_{1,2}}$, $a_{3,4} = i\sqrt{(E_{3,4} + |\delta|)/E_{3,4}}$, $b_{3,4} = \sqrt{(E_{3,4} - |\delta|)/E_{3,4}}\,\mathrm{sgn}(Ak \mp \gamma)$ for $\delta > 0$ and $a_{1,2} = -ib_{1,2}$, $b_{1,2} = ia_{1,2}$, $a_{3,4} = ib_{3,4}$, and $b_{3,4} = -ia_{3,4}$ for $\delta < 0$; $k = |\boldsymbol{k}|$, and φ is the polar angle of the wave vector $\boldsymbol{k}$, $e^{i\varphi} = k_+/k$. The coefficients a_j and b_j are defined in such a way that the wave functions (4) are continuous in $\boldsymbol{k}$ space.

The electron dispersion (3) is shown in Fig. 1. In the structure of the critical thickness the spectrum consists of two Dirac cones shifted vertically with respect to each other by $2|\gamma|$. At $d \neq d_c$, the gap of $2|\delta|$ opens in the spectrum at the wave vector $k_0 = |\gamma/A|$ and the system behaves as an insulator. The topological class of the insulator is determined by the sign of δ, similarly to the model where interface inversion asymmetry is neglected [8]. To confirm this, we calculate the $\mathbb{Z}_2$ topological index ν following the procedure described in Ref. [1]. The index ν is determined by the quantities $\zeta(\boldsymbol{\Lambda}_\alpha)$ ($\alpha = 1 \ldots 4$) calculated at four certain points of the Brillouin zone $\boldsymbol{\Lambda}_\alpha$ which are invariant with respect to the time inversion, $(-1)^\nu = \prod_\alpha \zeta(\boldsymbol{\Lambda}_\alpha)$. We find that

$$\zeta(\boldsymbol{k} = \mathbf{0}) = \lim_{\boldsymbol{k}\to\mathbf{0}} \frac{\mathrm{Pf}[\langle\Psi_i(\boldsymbol{k})|\Theta|\Psi_j(\boldsymbol{k})\rangle]}{\sqrt{\det[\langle\Psi_i(\boldsymbol{k})|\Theta|\Psi_j(\boldsymbol{k})\rangle]}} = \mathrm{sgn}\,\delta, \tag{5}$$

where the indices i and j run over the occupied branches 1 and 2, Θ is the operator of time inversion, and $\mathrm{Pf}[A]$ is the Pfaffian of the matrix A. All other $\zeta(\boldsymbol{\Lambda}_\alpha)$ are determined by the wave functions at the Brillouin zone edge and are unlikely to be affected by a small change of δ. Thus, we conclude that the topological transition occurs at $\delta = 0$: The QW structures with $d < d_c$ and $d > d_c$ belong to trivial and topological two-dimensional insulators, respectively. In the phase of a topological insulator, one expects the formation of helical edge states leading to the quantum spin Hall effect and conductivity quantization [9], although the electron structure of the edge states is modified by strong interface-induced coupling.

The large anticrossing of the $E1$ and $HH1$ subbands at $\boldsymbol{k} = \mathbf{0}$ revealed in the atomistic calculations indicates that the subband mixing mainly originates from the interface inversion asymmetry related to the anisotropy of chemical bonds. Since the $E1$ subband is formed from the electron and light-hole basis functions and the $HH1$ subband is of the heavy-hole type [see Eq. (1)], they are efficiently coupled due to heavy-hole–light-hole mixing at the interfaces, the effect known for zinc-blende-lattice QW structures [14–16,24,25]. This short-range mixing can be modeled by introducing interface terms to the effective Luttinger Hamiltonian which takes into account the low spatial symmetry of individual interfaces. The additional terms related to the left (L) and right (R) interfaces have the form $V_{L,R} = \pm\hbar^2 t_{l\text{-}h}/(\sqrt{3}a_0 m_0)\{J_x J_y\}_s \delta(z - z_{L,R})$, where $t_{l\text{-}h}$ is the (real) mixing constant, a_0 is the lattice constant, m_0 is the free electron mass, $\{J_x J_y\}_s = (J_x J_y + J_y J_x)/2$, J_x and J_y are the matrices of the angular momentum $3/2$, and $z_{L,R}$ are the interface positions. The terms lead to the coupling of the $E1$ and $HH1$ subbands with the parameter

$$\gamma = \frac{\hbar^2 t_{l\text{-}h}}{2a_0 m_0}\left[f_3(z_R) f_4(z_R) - f_3(z_L) f_4(z_L)\right]. \tag{6}$$

Since the envelope functions $f_3(z)$ and $f_4(z)$ have opposite parities, the parameter γ is nonzero. Comparing the results of atomistic calculation with the $\boldsymbol{k}\cdot\boldsymbol{p}$ theory we obtain $t_{l\text{-}h} \approx 1.5$. Extrapolation to $HgTe/Cd_{0.7}Hg_{0.3}Te$ QWs, the structures commonly used in experiment [9,12,13], gives $t_{l\text{-}h} \approx 1.1$ and $2|\gamma| = 10$ meV.

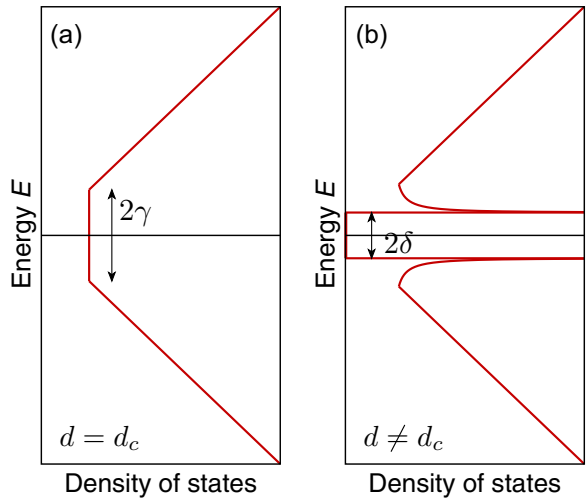

FIG. 4. (Color online) Sketch of the density of states in HgTe/CdTe QWs of the (a) critical and (b) close-to-critical thicknesses.

The splitting of Dirac states may affect many phenomena, including weak localization, Shubnikov–de Haas oscillations and the quantum Hall effect, spectra of THz radiation absorption, spin-flip Raman scattering, etc. The basic characteristic of electron systems is the single-particle density of states

$$\rho(E) = \sum_{l,\boldsymbol{k}} \delta[E - E_l(\boldsymbol{k})]\,. \tag{7}$$

For the QW system under study, it has the form

$$\rho(E) = \frac{|E|}{\pi A^2} \begin{cases} 0, & \text{if } |E| \leqslant |\delta|, \\ |\gamma|/\sqrt{E^2 - \delta^2}, & \text{if } |\delta| < |E| \leqslant \sqrt{\gamma^2 + \delta^2}, \\ 1, & \text{if } |E| > \sqrt{\gamma^2 + \delta^2}. \end{cases}$$

Figure 4 illustrates the density of states versus electron energy for QWs of critical and close-to-critical thicknesses. The gapless structure behaves as a two-dimensional semimetal with a finite density of states in the whole energy range [Fig. 4(a)]. The density of states linearly scales with the energy $\rho(E) = |E|/(\pi A^2)$ at $|E| > |\gamma|$ and is energy independent, $\rho(E) = |\gamma|/(\pi A^2)$, at $|E| < |\gamma|$. In the latter region, electrons and holes coexist and the conductivity is bipolar. In QWs of close-to-critical thicknesses [Fig. 4(b)], the density of states has a gap of $2|\delta|$ and van Hove singularities at $E = \pm\delta$.

The splitting of Dirac cones leads to a beating pattern in the Shubnikov–de Haas oscillations as well as splitting of the absorbance peak in experiments on cyclotron resonance. The peak positions are determined by the effective cyclotron masses $m_l = \hbar^2 k/(dE_l/dk)$. In an n-doped structure with a Fermi energy E_F, one can expect splitting of the resonant line into two components, their positions at $E_F \gg |\gamma|$ being determined by the effective masses $m_{3,4} = (\hbar/A)^2(E_F \pm \gamma)$.

The energy spectrum can be also studied by means of optical spectroscopy. For direct optical transitions between occupied and empty states, the QW absorbance at the normal incidence

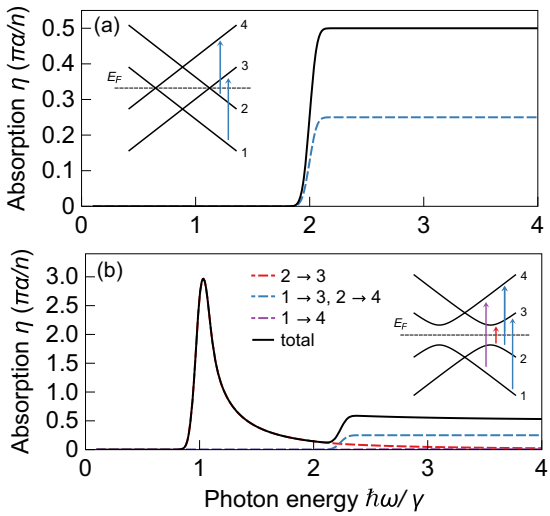

FIG. 5. (Color online) Photon energy dependence of the QW absorbance for structures of (a) the critical thickness $\delta = 0$ and (b) the close-to-critical thickness $\delta = 0.5\gamma$. Dashed curves show partial contributions to the absorbance. The inset sketches the energy spectrum and allowed optical transitions. The steep spectral edges are smoothed by convoluting the spectra with the Gaussian function with a standard deviation of 0.05γ.

of radiation is given by

$$\eta = \frac{4\pi^2\alpha\hbar}{\omega n_\omega} \sum_{l,m,\boldsymbol{k}} |\boldsymbol{e}\cdot\boldsymbol{v}_{ml}|^2\, \delta(E_m - E_l - \hbar\omega), \tag{8}$$

where α is the fine-structure constant, ω is the light frequency, n_ω is the refractive index of the medium, $\boldsymbol{e}$ is the (complex) unit vector of the light polarization, and $\boldsymbol{v}_{ml} = \hbar^{-1}(\partial H/\partial \boldsymbol{k})_{ml}$ is the matrix element of the velocity operator. We consider undoped QW structures where optical transitions can occur between the occupied branches 1 and 2 and the empty branches 3 and 4 of the energy spectrum [see the insets in Figs. 5(a) and 5(b)]. For normally incident radiation, the QW absorbance is independent of the light polarization and has the form

$$\eta = \frac{\pi\alpha A^2}{\hbar\omega n_\omega} \sum_{\substack{l=1,2 \\ m=3,4}} \sum_{k_t} \frac{k_t\, f_{ml}(k_t)}{|dE_m/dk - dE_l/dk|_{k=k_t}}, \tag{9}$$

where k_t is the wave vector at which the optical transitions between the branches l and m occur and is found from the equation $E_m(k_t) - E_l(k_t) = \hbar\omega$, and $f_{ml}(k)$ are the dimensionless functions defined by $f_{ml}(k) = (\hbar/A)^2|\boldsymbol{e}\cdot\boldsymbol{v}_{ml}|^2$. Straightforward calculations yield

$$f_{41} = \frac{\delta^2}{E_4^2}, \quad f_{32} = \frac{\delta^2}{E_3^2},$$
$$f_{31} = f_{42} = \frac{1}{2}\left(1 - \frac{A^2k^2 - \gamma^2 + \delta^2}{E_1 E_3}\right). \tag{10}$$

Figures 5(a) and 5(b) demonstrate the photon energy dependence of the QW absorbance for structures of critical and close-to-critical thicknesses. In a structure with two split Dirac cones [Fig. 5(a)], the absorption spectrum has a steplike shape with the edge at $\hbar\omega = 2|\gamma|$, although there is no band gap in the

energy spectrum. Such a behavior is dictated by the selection rules and energy conservation law: Direct optical transitions in QWs of critical thickness are allowed only between the branches $1 \to 3$ and $2 \to 4$ and these transitions can occur at $\hbar\omega \geqslant 2|\gamma|$. In QWs of noncritical thickness [Fig. 5(b)], the branches 2 and 3 anticross at a finite wave vector, and direct optical transitions between them become allowed. It leads to the emergence of an additional sharp band in the absorption spectrum at $\hbar\omega = 2|\delta|$. The spectral shape of this absorption band is determined by the van Hove singularities in the density of states.

To summarize, we have described the splitting of Dirac states in HgTe/CdTe quantum wells of critical and close-to-critical thicknesses. In structures of critical thickness, the splitting between the Dirac cones reaches a value of 15 meV and is dominated by symmetry-enforced light-hole–heavy-hole mixing at the quantum well interfaces. These structures behave as a two-dimensional semimetal with a nonvanishing density of states in the whole energy range. In quantum wells of close-to-critical thicknesses, a gap opens at a finite in-plane wave vector, which leads to the emergence of extremum circles in the electron dispersion and corresponding van Hove singularities in the density of states. We have also discussed the consequences of level mixing on the optical and transport properties that await testing.

Financial support by the RFBR, RF President Grants No. MD-3098.2014.2 and No. NSh-1085.2014.2, EU project SPANGL4Q, and the "Dynasty" Foundation is gratefully acknowledged. Work at the University of Colorado, Boulder by A.Z. was supported by the US Department of Energy, Office of Science, Basic Energy Science, Materials Sciences and Engineering Division under Contract No. DE-FG02-13ER46959 to the University of Colorado.

[1] M. Z. Hasan and C. L. Kane, Rev. Mod. Phys. **82**, 3045 (2010).
[2] X.-L. Qi and S. C. Zhang, Rev. Mod. Phys. **83**, 1057 (2011).
[3] Y. Xia, D. Qian, D. Hsieh, L. Wray, A. Pal, H. Lin, A. Bansil, D. Grauer, Y. S. Hor, R. J. Cava, and M. Z. Hasan, Nat. Phys. **5**, 398 (2009).
[4] Y. Tanaka, Z. Ren, T. Sato, K. Nakayama, S. Souma, T. Takahashi, K. Segawa, and Y. Ando, Nat. Phys. **8**, 800 (2012).
[5] M. I. Dyakonov and A. V. Khaetskii, Pis'ma Zh. Eksp. Teor. Fiz. **33**, 115 (1981) [JETP Lett. **33**, 110 (1981)].
[6] C. Brüne, C. X. Liu, E. G. Novik, E. M. Hankiewicz, H. Buhmann, Y. L. Chen, X. L. Qi, Z. X. Shen, S. C. Zhang, and L. W. Molenkamp, Phys. Rev. Lett. **106**, 126803 (2011).
[7] D. A. Kozlov, Z. D. Kvon, E. B. Olshanetsky, N. N. Mikhailov, S. A. Dvoretsky, and D. Weiss, Phys. Rev. Lett. **112**, 196801 (2014).
[8] B. A. Bernevig, T. L. Hughes, and S. C. Zhang, Science **314**, 1757 (2006).
[9] M. König, S. Wiedmann, C. Brüne, A. Roth, H. Buhmann, L. W. Molenkamp, X.-L. Qi, and S. C. Zhang, Science **318**, 766 (2007).
[10] J.-W. Luo and A. Zunger, Phys. Rev. Lett. **105**, 176805 (2010).
[11] L. G. Gerchikov and A. V. Subashiev, Fiz. Tekh. Poluprovodn. **23**, 2210 (1989) [Sov. Phys. Semicond. **23**, 1368 (1989)].
[12] B. Büttner, C. X. Liu, G. Tkachov, E. G. Novik, C. Brüne, H. Buhmann, E. M. Hankiewicz, P. Recher, B. Trauzettel, S. C. Zhang, and L. W. Molenkamp, Nat. Phys. **7**, 418 (2011).
[13] P. Olbrich, C. Zoth, P. Vierling, K.-M. Dantscher, G. V. Budkin, S. A. Tarasenko, V. V. Belkov, D. A. Kozlov, Z. D. Kvon, N. N. Mikhailov, S. A. Dvoretsky, and S. D. Ganichev, Phys. Rev. B **87**, 235439 (2013).
[14] E. L. Ivchenko, A. Yu. Kaminski, and U. Rössler, Phys. Rev. B **54**, 5852 (1996).
[15] O. Krebs, D. Rondi, J. L. Gentner, L. Goldstein, and P. Voisin, Phys. Rev. Lett. **80**, 5770 (1998).
[16] R. Magri and A. Zunger, Phys. Rev. B **62**, 10364 (2000).
[17] X. Dai, T. L. Hughes, X.-L. Qi, Z. Fang, and S. C. Zhang, Phys. Rev. B **77**, 125319 (2008).
[18] M. König, H. Buhmann, L. W. Molenkamp, T. L. Hughes, C.-X. Liu, X. L. Qi, and S. C. Zhang, J. Phys. Soc. Jpn. **77**, 031007 (2008).
[19] R. Winkler, L. Y. Wang, Y. H. Lin, and C. S. Chu, Solid State Commun. **152**, 2096 (2012).
[20] L. Weithofer and P. Recher, New J. Phys. **15**, 085008 (2013).
[21] G. M. Minkov, A. V. Germanenko, O. E. Rut, A. A. Sherstobitov, S. A. Dvoretski, and N. N. Mikhailov, Phys. Rev. B **89**, 165311 (2014).
[22] See Supplemental Material at http://link.aps.org/supplemental/10.1103/PhysRevB.91.081302 for details of the tight-binding calculations.
[23] J. Ludwig, Yu. B. Vasilyev, N. N. Mikhailov, J. M. Poumirol, Z. Jiang, O. Vafek, and D. Smirnov, Phys. Rev. B **89**, 241406(R) (2014).
[24] A. A. Toropov, E. L. Ivchenko, O. Krebs, S. Cortez, P. Voisin, and J. L. Gentner, Phys. Rev. B **63**, 035302 (2000).
[25] M. V. Durnev, M. M. Glazov, and E. L. Ivchenko, Phys. Rev. B **89**, 075430 (2014).